Structural and electronic properties of Ag-Pd superlattices

Matthieu J. Verstraete*
Unité de Physico-Chimie et de Physique des Matériaux (PCPM), Université Catholique de Louvain, 1 Croix du Sud, B-1348 Louvain-la-Neuve, Belgium

Jacques Dumont and Robert Sporken
Laboratoire de Physique des Matériaux Electroniques (LPME), Facultés Universitaires Notre-Dame de la Paix, Namur, Belgium

R. L. Johnson
Institut für Experimentalphysik, Universität Hamburg, Luruper Chausee 149, 22761 Hamburg, Germany

Frédéric Wiame
Laboratoire pour l'utilisation du rayonnement électromagnétique (LURE), Université Paris-Sud, F-91405, Orsay, France

Kristiaan Temst and Johan Swerts
Laboratorium voor Vaste-Stoffysica en Magnetisme (LVSM), Katholieke Universiteit Leuven, Celestijnenlaan 200D, B-3001 Heverlee, Belgium

Frédéric Mirabella and Jacques Ghijsen
Laboratoire Interdisciplinaire de Spectroscopie Electronique (LISE), Facultés Universitaires Notre-Dame de la Paix, Namur, Belgium

Xavier Gonze
Unité de Physico-Chimie et de Physique des Matériaux (PCPM), Université Catholique de Louvain, 1 Croix du Sud, B-1348 Louvain-la-Neuve, Belgium

(Received 4 December 2003; revised manuscript received 17 February 2004; published 23 November 2004)

The electronic structure of silver-palladium heterostructures is investigated, both experimentally and through *ab initio* calculations. Synchrotron-radiation induced photoelectron spectroscopy characterizations of the work function and the valence band structure are compared to and explained by calculations of slab and bulk heterostructures. Work functions and equilibrium geometries are shown to be in agreement with synchrotron-radiation induced photoelectron spectroscopy, x-ray diffraction and scanning tunneling microscopy measurements. Further insight into the differing behavior of the two terminating metal surfaces is extracted from the calculations.

DOI: 10.1103/PhysRevB.70.205427 PACS number(s): 71.20.Be, 73.20.At, 81.15.Cd, 61.10.Eq

I. INTRODUCTION

The characterization of silver/palladium systems has been ongoing since the 1970s, on experimental and theoretical fronts. Both metals are used as catalysts, and their surfaces present many interesting technological characteristics. Recently, interest in Ag/Pd alloys has greatly increased, with applications in domains that range from dentistry[1,2] to liquid crystal display screens[3] (in particular with Ag/Pd nanoparticles) to hydrogen separation and storage.[4–6] Ag/Pd-alloy multilayers are also deposited on substrates and made into thin films for catalytic purposes and hydrogen applications. Theoretical work on the numerous possible alloys is sustained.[7–10]

Heterostructures built from alternating layers of deposited Ag and Pd have been studied experimentally in the past few years using x-ray diffraction (XRD), synchrotron-radiation induced photoelectron spectroscopy (SR-PES), atomic force microscopy, scanning tunneling microscopy (STM) and many other techniques.[11–21] At room temperature Ag and Pd have been described as growing layer by layer on each other. Standard properties are still controversial, as both metals have been observed to grow on the other with their own lattice parameter as well as pseudo-morphically.[14,15,22] In superlattices, root-mean-squared interface roughness can be lowered to about 1 atomic layer[21] but interdiffusion occurs above 200 °C.[13,16,18–21]

Much is known about thick multilayers of Ag and Pd, about the epitaxial growth of the metals on each other, and about their interdiffusion and alloy formation. The Ag/Pd system looks like the ideal superlattice: perfectly layered when grown at room temperature and without any interdiffusion. Nevertheless, until now, few theoretical or *in situ* studies have been carried out on the growth mechanisms and electronic structure of Ag/Pd superlattices.

In this article, we present first-principles density functional theory (DFT) calculations of a series of Ag/Pd heterostructures with (111) orientation, and the experimental characterization of these systems by STM and SR-PES. We will focus mainly on the calculation of the electronic structure and the characterization of the superlattice; specifics of the experimental aspects of its growth will be presented in a future publication.[23] The terms heterostructure and superlattice will be used interchangeably to denote the crystalline

superposition of atomic monolayers of Ag and Pd. Experimentally, the term "monolayer" (ML) will denote the amount of Ag or Pd atoms needed to build 1 ML of these elements on their own bulk lattice parameter. On a (111) surface, this gives one uniform layer of a triangular lattice, if one discounts changes in in-plane lattice parameters. In the calculations, only one unit cell, and hence one lattice parameter, is used at a time, and therefore monolayers are always ideal and uniform.

In the following Sec. II we describe the theoretical and experimental methods used to characterize Ag/Pd superlattices. Sec. III describes the geometrical crystalline properties of the superlattices, and compares calculated and experimental lattice constants. Section IV follows where the electronic structure of the metallic surfaces is analyzed. Section V contains our conclusions.

II. METHOD

A. Computational methods

First-principles DFT calculations are performed using the ABINIT[24–26] plane-wave (PW) code. Norm-conserving, separable, Trouiller-Martins pseudopotentials are used to describe the interactions between atomic cores and valence electrons. Calculations are performed in the generalized-gradient approximation (GGA) of Perdew, Burke, and Ernzerhof.[27] A PW kinetic energy cutoff of 50 Ha and a *k*-point grid of $4\times4\times4$ *k* points with a smearing width of 0.02–0.03 Ha are needed to converge the cubic lattice parameter to within 0.01%. Our slab calculations are done in a hexagonal cell to accomodate the (111) surface we wish to calculate. In this case the *k*-point grid converges more slowly, and the *k*-point grids are less symmetrical. For palladium in particular, the ideal c/a ratio of $\sqrt{6}$ is badly reproduced if the fcc grid is simply transferred to the hexagonal cell. We find that tight convergence necessitates a $10\times10\times10$ grid of *k* points in the hexagonal cell. All calculations have been performed with the tight grid in hexagonal cells. The in-plane hexagonal lattice parameter is $a_{cubic}/\sqrt{2}$.

The pseudopotentials are tested on bulk silver and palladium. The GGA cubic lattice constants obtained are 4.17 and 3.93 Å, i.e., 2.2% and 1.2% above the 4.09 and 3.89 Å experimental values, respectively. The in-plane hexagonal lattice parameters are then 2.95 and 2.78 Å, resp. Atomic positions and lattice parameters are relaxed using a Broyden algorithm.[28,29] Several physical quantities are calculated *ab initio* and can be compared to experiment.

1. Work functions

A by-product of the DFT electronic calculation is the total external potential for the electrons. The difference between the value of the external potential in vacuum and the Fermi level (inside the slab) gives the DFT work function $\phi = v_{\text{vacuum}} - E_{\text{Fermi}}$. It has been shown that the calculation of the work function can be facilitated with a correction term. We test this method[30] in our metallic systems in Sec. III.

2. Ground state geometries

Specific systems of interest are allowed to relax to their equilibrium geometries. This allows us to compare the predicted interlayer distances and lattice parameters in heterostructures with experimental values.

3. Densities of states

The density of states (DOS) is obtained by sampling the Brillouin zone with a large number of *k* points. The (discrete) states we obtain are broadened in energy with a Gaussian of width 0.015 (Ha), or integrated using the tetrahedron method.

4. Surface energies

The energy needed to create a surface can be calculated by subtracting the energy of a slab system (with two surfaces) from the energy of the equivalent number of bulk atoms, and dividing by two. An analogous procedure can be employed for interface energies.

5. The systems

We consider three types of systems in our calculations. Pure slabs of Ag or Pd (111) are used to verify the accuracy of the method for calculating work functions. Then, infinitely repeated heterostructures are used to model $(Ag_3Pd_3)_N$ crystalline structures (we will denote by Ag_nPd_m a heterostructure consisting of *n* monolayers of silver and *m* of palladium). Finally, the surfaces of these heterostructures are modeled using slabs of $Ag_mPd_3Ag_m$ and $Pd_mAg_3Pd_m$ with $m=1,2,3$ ML and seven layers of vacuum, and their work functions are calculated. For slab systems a $10\times10\times1$ *k*-point grid was used throughout.

B. Experimental methods

Ag and Pd are evaporated on a Muscovite mica substrate. The freshly cleaved Muscovite mica is first annealed to 200 °C under ultrahigh vacuum (UHV) before a Ag layer of at least 3000 Å is deposited at rates of 30 Å/s from a resistively heated tungsten boat. The films are annealed for more than 1 h to improve their short-range order. The Ag buffer layers being prepared in a separate chamber are exposed to air before analysis. To remove the adsorbed contamination, the samples are annealed again to 200 °C after introduction in the UHV analysis systems. Auger electron spectroscopy shows that this procedure gives clean Ag surfaces. The Ag and Pd layers were evaporated from 99.99% pure materials. During deposition the substrate was left at room temperature. Ag and Pd were evaporated at 0.01 and 0.002 Å/s, respectively. We check the thickness of the layers with a quartz crystal thickness monitor. This method has the advantage of being very accurate and therefore allows a high reproducibility in the thickness of the layer deposited. The method can sometimes fail to give precise absolute values of these thickness. A careful analysis of the STM images at the earliest stages of the deposition steps showed however that our quartz microbalance was properly calibrated. The pressure is about 2.5×10^{-10} Torr before the evaporations, and about 2×10^{-8} Torr (resp. 2×10^{-9} Torr) during the growth of the thick Ag layer (resp. the superlattice).

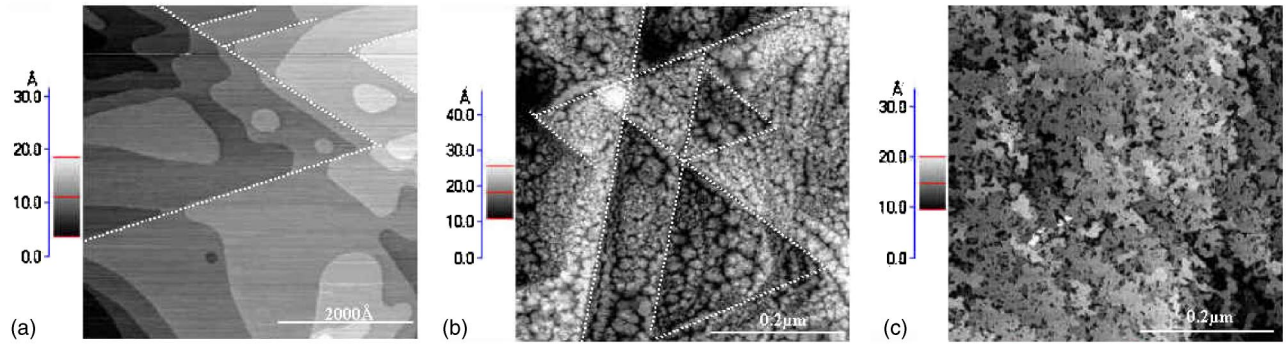

FIG. 1. (a) STM image of the Ag/mica buffer layer. Large (>200 nm) atomically flat terraces are visible. (b) STM image of 3 ML of Pd deposited on the buffer Ag. Pd growth is columnar but fcc stacking and the (111) orientation are preserved: the dashed lines are a guide for the eye, following step edges on the substrate. (c) STM image of 3 ML of Ag deposited on the previous 3 ML of Pd.

The SR-PES experiments give us access to the work functions of the different surfaces, and to the valence-band density of states. They were carried out on the Flipper II (E1) beamline in HASYLAB. The photon energy chosen for our experiments was 20 eV. The typical resolution of the spectrometer, described in detail in the literature,[31] is 0.1 eV with a 50 μm entrance slit and the basic vacuum of the system is on the order of 2×10^{-10} Torr.

Another UHV system (base pressure 1×10^{-10} Torr) is used for STM (a VP2 from Park Scientific Instruments), Auger electron spectroscopy and low-energy electron diffraction. All STM images are recorded in constant current mode with electrochemically etched and vacuum-annealed W tips. All images are raw data except for the removal of a linear background in order to take into account the piezoelectric drift perpendicular to the surface. After growth and STM analysis, two samples were analyzed *ex situ* by XRD to determine their crystalline structure. The x-ray diffraction measurements were carried out on a Rigaku diffractometer. All experiments were performed in the Bragg-Brentano ($\theta-2\theta$) geometry using Cu $K\alpha$ radiation [wavelength 0.154 (nm)] and a postsample crystal monochromator. The diffraction patterns were collected with a step size of 0.01°.

III. GEOMETRICAL PROPERTIES OF THE SUPERLATTICES

A. STM results

A silver (111) buffer layer grown on a mica substrate is shown in Fig. 1(a). The surface is atomically flat over terraces larger than 0.5 μm (see figure). The threefold symmetry of the step edges arises from the (111) orientation of the system. The terraces are separated by monoatomic steps having a height of 2.4±.1 Å. The tabulated distance between Ag(111) planes is 2.36 Å, so this value confirms the proper calibration of our scanner in the direction normal to the surface. As seen in Fig. 1(b), the growth of 3 ML of Pd on this substrate proceeds in columns separated by grooves about 3 ML deep. Fortunately, due to the lower surface energy of silver, 3 ML of Ag grown on this columnar structure appear to reconstruct the whole system giving rise to atomically flat layers that can be alternated in a superlattice without alloying or intermixing Fig. 1(c). Further growth of Pd on this layer is two dimensional and so is the growth of the whole superlattice.

B. *Ab initio* results

The superlattices studied experimentally contain one or more units of (Ag_3Pd_3) deposited on the Ag buffer layer, and are terminated by Ag_3 or Pd_3. Since the addition of large numbers of such units to our calculations would have been prohibitive in computational terms, we exploit the inherently periodic nature of PW calculations and calculate an infinite $(Ag_3Pd_3)_\infty$ system, using a $10\times10\times4$ k-point grid. The atomic positions and lattice parameters of $(Ag_3Pd_3)_\infty$ are first allowed to relax completely, until the forces are below 9×10^{-5} eV/Å and the pressure on the system is lower than 1×10^{-4} (GPa). The resulting lattice parameter in the close-packed plane is 2.85 Å, an intermediate value between those for Pd (2.78 Å) and Ag (2.95 Å). This result is coherent with experimental observations of both pseudo-morphic growths of Ag on Pd and vice versa. The interplane distances between Ag-Ag, Ag—Pd, and Pd—Pd, are, respectively 2.48, 2.34, and 2.24 Å.

Finally, we calculate an interface energy which is less than 10 meV/unit cell, i.e., 0 within our calculational precision. Such a low interface energy, in the ambient temperature range considered, makes the growth of the heterostructures energetically plausible. To determine which of the pseudo-morphic growths is more favorable, we perform simulations of the same infinite heterostructure, imposing the in-plane lattice parameter to be that of Ag and then Pd, and relaxing the atomic positions and the third dimension of the unit cell. With the Ag lattice parameter, the interface energy is 135 meV/unit cell, whereas with the Pd lattice parameter the value is 91 meV/unit cell. The pseudo-morphic growth of Ag on Pd thus appears favored, but still less so than the intermediate relaxed lattice parameter. The Ag—Pd interlayer distance is 2.28 and 2.38 Å for the Ag or Pd in-plane lattice parameter, respectively.

C. XRD measurements

The XRD diagram of $(Ag_3Pd_3)_{13}$ and $(Ag_3Pd_3)_{22}$ superlattices grown in different UHV chambers is shown in Fig. 2.

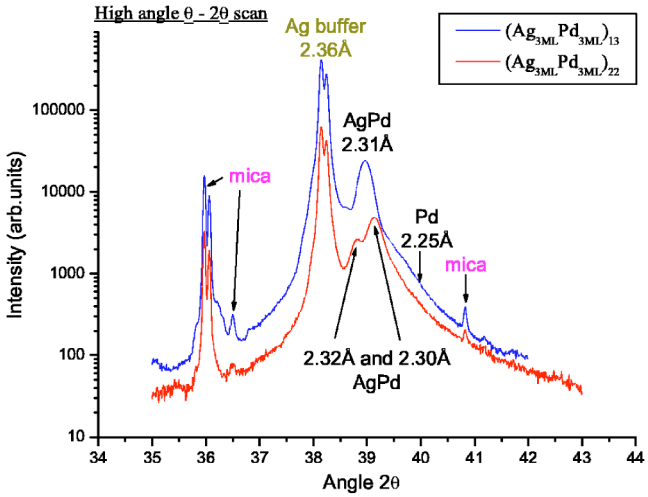

FIG. 2. X-ray diffraction diagrams for the completed Ag/Pd superlattice, as a function of 2θ. The characteristic peaks of Ag and mica can be seen, along with additional peaks for the superlattice around 2.30 Å. The two diagrams correspond to different deposition chambers, and confirm the reproducible and controlled structure of the superlattices.

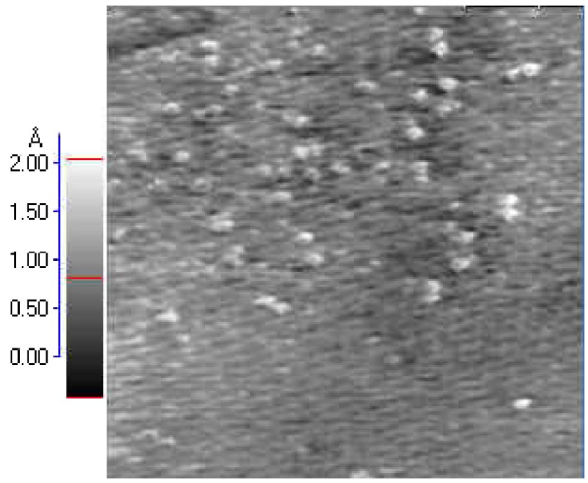

FIG. 3. Silver (3 ML) on 16 ML of palladium. The Pd atoms substituted in the surface are visible and appear 0.9 Å higher, in agreement with the Ag/Pd alloy results in Ref. 33. (I_{tunnel}=12 nA, V_{sample}=1 V).

X-ray diffraction gives us access to interlayer distances in the heterostructure but also to the periodicity in the superlattice. Unfortunately in our case the information relative to the superlattice is superimposed on those from the mica substrate and from the Ag buffer layer. The important peaks are located around 36°, 38°, 39°, and 41°. A reference mica sheet shows doubled peaks at 36°, 36.5°, and 41°.

The peaks around 39° are related to an average superlattice spacing of 2.31 Å which is between the Pd (111) lattice spacing of 2.25 Å and Ag (111) lattice spacing of 2.36 Å (shown by the peak of the Ag buffer layer at 38.1°). This means that we have either a Ag/Pd solid solution or that the superlattice has intermediate lattice spacings due to the growth of the superlattice. The fact that the peak at 39° is split into two features on the lower curve supports the second hypothesis: in a random solid solution the Ag-Pd distances would be averaged out and would give a single wide peak. As stated in the introduction, other studies found interdiffusion to be negligible below 200 °C.[13,16,18–21] However, this also implies that the heterostructures are not uniform across the whole surface and/or across the whole depth. In order to observe several peaks, part of the heterostructure must have a slightly different sequence of layers, but still be uniform and crystalline enough to give a diffraction peak. Our claim that the system stays a heterostructure, and that intermixing of Ag and Pd is minor, is further confirmed by the work function in Sec. IV.

As mentioned above, the calculated heterostructures confirm that the pseudo-morphic growth of Ag on Pd is favored, but that an in-plane lattice parameter between that of Pd and that of Ag would be even better. The x-ray peaks around 2.31 Å correspond to the distance between Ag and Pd layers (to within 1.5%) in the fully relaxed structure with an intermediate in-plane lattice constant. The Pd-Pd distance is 1.3% shorter than the bulk value, and can account for the shoulder around 40°. The Ag-Ag distance is 3% longer at 2.48 Å and is therefore very close to the mica peak around 36°. The Ag—Ag peak could be responsible for the shoulder at 36.2°, but to be certain new measurements would have to be carried out with a different substrate. The calculations of Lu, Wei, and Zunger[32] for a 50% Ag-Pd alloy give a (111) interlayer distance of 2.26 Å, significantly smaller than our 2.31 Å [despite the usual local density approximation underestimation of equilibrium distances in their case].

Although *ab initio* calculations and XRD results comfort the idea that the interfaces between Ag and Pd layers are abrupt, imperfections appear after several periods. Figure 3 shows bright atomic protrusions attributed to Pd atoms substituted in the Ag surface of $(Ag_3Pd_3)_3$/Ag/mica. Such chemical discrimination by STM was already observed on the (111) and (100) surfaces of Ag/Pd alloys by Wouda *et al.*[33] who found Pd atoms to be enhanced by 0.25 Å compared to Ag atoms.

To sum up, several indices confirm the construction of a Ag-Pd heterostructure with abrupt interfaces, but we cannot exclude the possibility of some intermixing between the two species. We will proceed to examine the rest of the properties of the system with the hypothesis of a regular crystalline heterostructure, adopting an intermediate in-plane lattice parameter simliar to the relaxed *ab initio* one.

IV. ELECTRONIC PROPERTIES OF THE SUPERLATTICES

A. Work function

1. Pure metals

Simulations of slabs with only one atomic species are used to validate our procedure for the determination of the work function and especially to examine the effect of two parameters, namely the in-plane lattice parameter and the thickness of the vacuum around the slab. The number of vacuum layers needed to isolate the slab from its images in neighboring cells is found to be about seven for both metals.

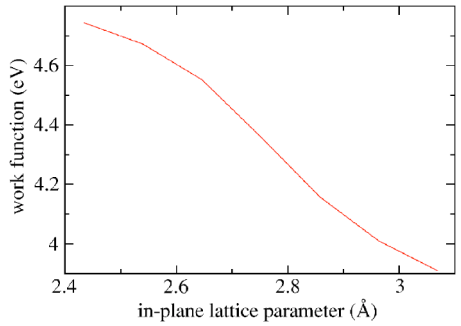

FIG. 4. Variation of the DFT work function with respect to the imposed lattice parameter, for a three layer slab of silver.

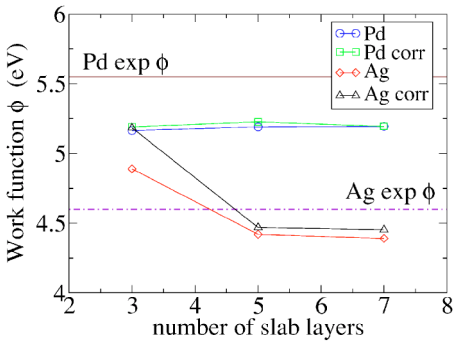

FIG. 5. Work function (V) as a function of the number of slab layers, with and without the correction described in the text a is fixed to its value for the calculated bulk material.

This corresponds to a distance between surfaces of about 16 Å.

The work function of a surface arises from the spill out of electrons into the vacuum. Therefore, it strongly depends on the lateral confinement of the electronic density and thus on the lattice parameter used for the slab calculation. Figure 4 shows the variation of the work function with the in-plane lattice parameter a, for fixed fictitious interlayer distances and three layers of silver (a sparser $4\times4\times1$ kpoint mesh is used for this qualitative example). The work function decreases with the lattice parameter. Relaxing the three-layer slab gives a lattice parameter of 2.71 Å, much smaller than the bulk value of 2.97 Å and giving a difference of more than 0.4 eV in the work function due to lattice parameter.

If the lattice parameter is set to the bulk value, and the distance between the central and surface layers is increased, the work function increases, as electrons on the surface are pulled in by the sublayer. For surface-layer distances between ±5%, which are observed when the slabs are relaxed, the work function varies linearly by ±0.2 eV. Surface relaxation effects are thus also important for the calculation of work functions, but the effect is smaller than that of the in-plane lattice parameter, and for small surface relaxations it is close to the inherent error of both the calculations and experiment, which is around 0.1 eV.

Relaxing the lattice parameter for too thin a slab is meaningless, because it is too small to represent two independent silver surfaces properly. Therefore, and for the reasons exposed above, we must make a consistent choice of a value for a. This is needed in order to be able to compare the calculations with each other and with experiment. For the work function calculations in this section, we fix the in-plane lattice parameter for the slab to that found *ab initio* for bulk metals, i.e., 2.95 and 2.78 Å for Ag and Pd, respectively.

The work functions of Ag and Pd surfaces are calculated using progressively thicker slabs: as described above, in order to simulate a true surface, the outermost (surface) layers must be separated by a bulk-like region. We find that a total of five layers is sufficient for this purpose. The convergence is shown in Fig. 5 (Pd: circles and Ag: diamonds). From this calculation, the work functions we find for Ag and Pd are 4.4 and 5.2 V, respectively.

We also compare the standard method for calculating the work function with a correction used, e.g., in Ref. 30. The correction consists in aligning the potential in the slab with the corresponding potential in the bulk material, and using the position of the Fermi energy from the bulk to calculate the work function. The correction is the following:

$$\phi = v_{\text{vacuum}} - (v_{\text{slab}} + E_{\text{Fermi}}(\text{bulk}) - v_{\text{bulk}}), \qquad (1)$$

where v_{vacuum} is the potential in the vacuum, v_{slab} and v_{bulk} are the electronic potentials in the slab and in the bulk which we want to align, and E_{Fermi}(bulk) is the Fermi level calculated in the bulk. This should correct the position of the Fermi energy for the absence of bulk states in the slab. Provided the potential at the surface and in vacuum is already well described, the work function should be correct with fewer layers of metal. The results, with and without the correction are shown in Fig. 5. The convergence of ϕ is not improved by the correction: five layers of metal are still needed to converge the work function to within 0.1 eV. However, the converged values obtained with the correction are between 0.05 and 0.1 eV higher, and thus closer to the experimental data (thick lines). Either the proposed explanation for the correction is incorrect, or the convergence of the slab potential to the true bulk potential is excruciatingly slow.

Using photoelectron spectroscopy, the work function of a material can easily be obtained from $\phi_m = h\nu - W$ where W is defined as the energy difference between the Fermi level and the cutoff energy of the spectrum. Our SR-PES measurements give work functions of 4.6 eV for the Ag buffer layer, and 5.6 eV for a three-layer deposit of Pd on the Ag surface. The experimental values for the work functions found in the literature are between 4.3 and 4.8 eV for Ag and between 5.2 and 5.6 eV for Pd (cf. references cited in Ref. 34). The differences in the literature are mainly due to the crystallinity of the surface: the (111) face of fcc metals being the closest packed, it has the highest work function, and any defect or disorder in the layer systematically lowers the work function. Our experimental values are in good agreement with the literature and confirm the quality of the orientation of the surfaces already proven with STM. The calculations model perfect (111) surfaces; hence, we can compare the ϕ obtained with our photoemission values. We find differences of 4% for Ag and 7% for Pd. Given the precision of $\sim$0.1 eV in the photoemission data, this confirms that our technique can provide quantitative information.

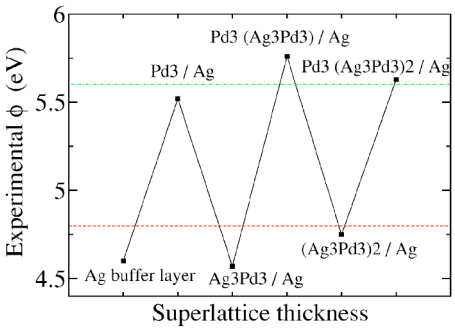

FIG. 6. Work functions (eV) of superlattices with 0, 1, and 2 (Ag_3Pd_3) blocks deposited on the Ag buffer layer, and the values for intermediate silver terminated heterostructures.

2. Heterostructures

Figure 6 shows the work function obtained between growth steps of a Ag_3Pd_3 superlattice after each deposition of three full layers of one metal. The resulting ϕ for 0, 1, and 2 depositions of (Ag_3Pd_3) vary only slightly from their bulk values as the superlattice is built up, and the fluctuations are probably due to the sample's surface topology on the micrometer scale, which changes the observed work function. If the growth allowed for significant amounts of intermixing, the work functions would be closer to the average of ϕ_{Ag} and ϕ_{Pd} which is not the case. Since this is true at each step, the fact that the work functions are saturated further comforts our hypothesis of a well defined superlattice with little mixing of Ag and Pd.

In order to model the heterostructure surfaces, we first consider slabs with central layers of one metal, sandwiched between by monolayers of the other metal, i.e., $Ag_1Pd_3Ag_1$, $Ag_2Pd_3Ag_2$, and $Ag_3Pd_3Ag_3$. The value of the lattice parameter is kept fixed to that of the infinite $(Ag_3Pd_3)_\infty$ heterostructure described above. Similarly, the Ag-Ag, Pd-Pd, and Ag-Pd interlayer spacings are taken from $(Ag_3Pd_3)_\infty$: in these slabs, the relaxation of the surface interlayer spacing is influenced mainly by the nature of the sublayer. Also, the slabs are too thin to be able to relax the surface-layer spacing reliably (and as mentioned above the effect of surface relaxation is weaker than that of the in-plane lattice parameter), so we keep the atomic positions fixed. The work functions of these slabs are given in Table I.

For both terminating metals, 2 ML give a slightly lower work function than 1 or 3 ML, by about 0.1 eV. This could be due to a charge transfer effect between the surface atoms and the "bulk" as observed for the case of Ni deposited on copper in Ref. 35. After only 1 or 2 ML, ϕ has already adopted its bulk value confirming the experimental results. This behavior arises from the strong screening in metals over the Thomas-Fermi screening length (on the order of a fraction of a monolayer).

TABLE I. Work functions for successive layers of Ag on a slab of $Pd_{3\ ML}$ and Pd on a slab of $Ag_{3\ ML}$.

System	ϕ (eV)	System	ϕ (eV)
$Ag_1Pd_3Ag_1$	4.51	$Pd_1Ag_3Pd_1$	5.30
$Ag_2Pd_3Ag_2$	4.42	$Pd_2Ag_3Pd_2$	5.16
$Ag_3Pd_3Ag_3$	4.46	$Pd_3Ag_3Pd_3$	5.14

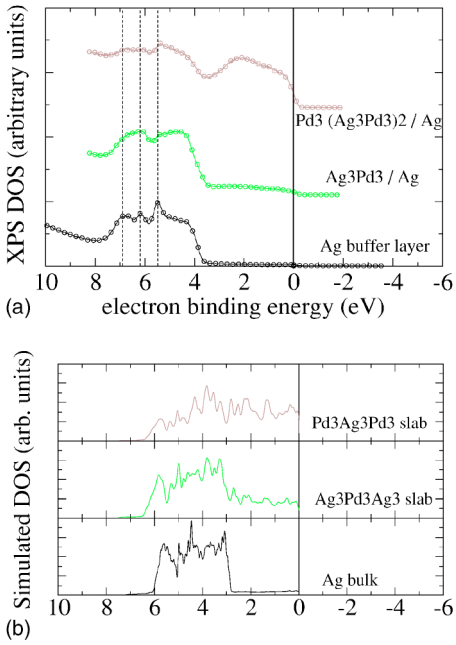

FIG. 7. Top: experimental (SR-PES) valence bands (circles). Bottom: calculated valence band DOS (lines) for Ag and Pd terminated superlattices.

B. DOS and valence bands

Finally, the density of states (DOS) is measured experimentally and calculated *ab initio*. SR-PES measurements give the valence band, i.e., the DOS of the occupied electron states, for the superlattices described above: units of (Ag_3Pd_3) terminating with Ag_3 or Pd_3. Simulations of bulk metals and slab heterostructures give the total DOS, with 4000 wave vectors in the bulk Brillouin zone and 100 wave vectors for the slabs. As SR-PES is a surface measurement, surface states, which are not present in our bulk calculations, will appear in the SR-PES DOS. In these circumstances, the calculation of a slab instead of a bulk system is necessary. Figure 7 top inset shows the valence bands obtained with SR-PES for (from bottom to top) the Ag buffer layer, Ag_3Pd_3 deposited on Ag, and $Pd_3(Ag_3Pd_3)_2$/Ag. Figure 7 bottom inset shows calculated DOS for (from bottom to top) Ag bulk metal, a $Ag_3Pd_3Ag_3$ slab, and a $Pd_3Ag_3Pd_3$ slab.

The shapes of the spectra agree qualitatively on a number of points. The three low-energy Ag peaks are present in all spectra [dashed lines in (a)], and the DOS remains much smaller in the Ag-terminated cases (reflecting the Ag *s* band). The Pd terminated DOS has a plateau (the Pd *d* band) between the Ag *d* band and the Fermi energy.

However, one cannot simply superpose the calculated DOS: the *ab initio* Ag *d*-band edge is around 3 eV, whereas the SR-PES spectra place it closer to 3.9 eV. Furthermore, the Ag bands extend down to 7 eV below the Fermi energy

in SR-PES, and only to 6 eV *ab initio*.

Lu, Wei, and Zunger also find a *d*-band edge around 3 eV for pure Ag and in Ag/Pd alloys, in their linear augmented plane wave calculations (Ref. 32), which confirms our DOS calculations. Experimentally, Coulthard and Sham find a Ag *d*-band edge between 4 and 3.5 eV experimentally by x-ray absorption near edge structure spectroscopy (Ref. 36). The error in the calculated values is probably caused by the error in the geometry. As shown in Ref. 32 for the case of Ag and Pd, both alone and in alloys, the lattice parameter can both change the bandwidth and shift the band structure: a 4% decrease in the lattice parameter for Ag gives a shift of the lower band edge 0.8 eV deeper, whereas the upper band edge is almost unchanged. Since our DFT lattice constants are only precise to within 3%, this can explain the bandwidth difference. The shape of the calculated DOS for the heterostructures is very similar to the partial DOS of Ag and Pd in Ag-Pd alloys, shown in Ref. 32 Lu, Wei, and Zunger explain this through the large charge transfer from Ag to Pd, which should carry over to the transfer between layers in our heterostructures.

Finally, the low-energy regions of the SR-PES spectra contain core states, which are not present in our pseudopotential calculation. This adds to the uncertainty on the low edge of the SR-PES *d* band, since the core states extend slightly beyond the *d*-band minimum.

Once again, the observation supports the hypothesis that the experimental sample is a Ag-Pd supperlattice, as opposed to a random alloy, which would not discriminate between Ag and Pd terminated surfaces: 1 or 2 ML of metal are enough to saturate the work function and DOS to their bulk values, but as there is only enough matter to build 3 ML, surface atoms of the other metal should be apparent, and their presence would be reflected in the work function and SR-PES DOS.

V. CONCLUSIONS

We have presented a combined experimental and numerical investigation of the electronic and crystalline structure of Ag/Pd superlattices. The two approaches agree qualitatively and quantitatively, and characterize the controlled growth of heterostructures with 3 ML of Ag alternating with 3 ML of Pd. The superlattice appears to adopt an in-plane lattice parameter which is intermediate between those of Ag and Pd, and preserves its crystallinity (determined by XRD or STM) even after several dozen ML. The calculated density of states for the valence band and the work functions agree with SR-PES measurements to within 0.2 eV. The work function saturates to its bulk value quickly, after only 1 or 2 ML of deposited metal, and the valence DOS is similarly characteristic of the last few ML. For Ag-terminated surfaces, the DOS around the Fermi level is small, corresponding to the *s* band of Ag, whereas for Pd-terminated surfaces the DOS is much higher (due to the Pd *d* band). A correction to the DFT calculation of the work function is tested and criticized. Further investigation is needed into the growth mechanism of the superlattices, both experimentally and theoretically. This work is ongoing, to explain and exploit the STM images taken in the course of the different growth phases: Pd deposited on the Ag substrate, then Ag on Pd, and finally Pd on the pseudo-morphic Ag.

ACKNOWLEDGMENTS

This work was supported by the Belgian Office for Scientific, Technical and Cultural Affairs (PAI 5.01), by the Belgian National Fund for Scientific Research (FNRS), and by FRFC Project No. 2.4556.99 and 1.5015.00 F. J.D. is supported by the FRIA and J.G. and X.G. are supported by the FNRS (Belgium).

*Electronic address: verstraete@pcpm.ucl.ac.be

[1] M. F. L. de Mele and G. Duffo, J. Appl. Electrochem. **32**, 157 (2002).
[2] J. Otulakowska and K. Jozwiak, J. Dent. Res. **80**, 1280 (2001).
[3] W. H. Lee, B. S. Cho, B. J. Kang, J. Y. Kim, J. G. Lee, C. O. Jeong, and Y. G. Kim, J. Korean Phys. Soc. **40**, 110 (2002).
[4] O. M. Lovvik and R. A. Olsen, J. Alloys Compd. **330**, 332 (2002).
[5] H. Amandusson, L. G. Ekedahl, and H. Dannetun, J. Membr. Sci. **193**, 35 (2001).
[6] S. Tosti, L. Bettinali, and V. Violante, Int. J. Hydrogen Energy **25**, 319 (2000).
[7] S. Müller and A. Zunger, Phys. Rev. Lett. **87**, 165502 (2001).
[8] I. A. Abrikosov, W. Olovsson, and B. Johansson, Phys. Rev. Lett. **87**, 176403 (2001).
[9] J. N. Keuler, L. Lorenzen, R. D. Sanderson, V. Prozesky, and W. J. Przybylowicz, Thin Solid Films **347**, 91 (1999).
[10] K. Kokko, R. Laihia, M. Alatalo, P. T. Salo, M. P. J. Punkkinen, I. J. Väyrynen, W. Hergert, and D. Kodderitzsch, Phys. Rev. B **60**, 4659 (1999).
[11] S. Kim and I. K. Schuller, Phys. Rev. B **58**, 2240 (1998).
[12] I. K. Schuller, S. Kim, and C. Leighton, J. Magn. Magn. Mater. **200**, 571 (1999).
[13] J. M. Guglielmacci and M. Gillet, Thin Solid Films **68**, 407 (1980).
[14] B. Eisenhut, J. Stober, G. Rangelov, and T. Fauster, Phys. Rev. B **47**, 12 980 (1993).
[15] G. N. Burland and P. J. Dobson, Thin Solid Films **75**, 383 (1981).
[16] K. Häupl and P. Wissmann, Thin Solid Films **174**, 105 (1989).
[17] G. C. Smith, C. Norris, C. Binns, and H. A. Padmore, J. Phys. C **15**, 6481 (1982).
[18] G. E. Henein and J. E. Hilliard, J. Appl. Phys. **54-2**, 728 (1983).
[19] T. Pienkos, L. Gladyszewski, D. Chocyk, and G. Gladyszewski, Mater. Sci. Eng., A **288**, 266 (2000).
[20] G. Gladyszewski, Mater. Lett. **13**, 287 (1992).
[21] K. Temst, M. J. Van Bael, C. Van Haesendonck, Y. Bruynseraede, D. G. de Groot, N. Koemann, and R. Griessen, Thin Solid Films **342**, 174 (1999).
[22] J. Dumont, J. Ghijsen, and R. Sporken, Surf. Sci. **507**, 234 (2002).

[23] J. Dumont, M. Verstraete, F. Wiame, F. Mirabella, J. Ghijsen, R. Sporken, and X. Gonze (unpublished).
[24] X. Gonze, J.-M. Beuken, R. Caracas, F. Detraux, M. Fuchs, G.-M. Rignanese, L. Sindic, M. Verstraete, G. Zerah, F. Jollet, M. Torrent, A. Roy, M. Mikami, Ph. Ghosez, J.-Y. Raty, and D. C. Allan, Comput. Mater. Sci. **25**, 478 (2002); ABINIT is a common project of the Université Catholique de Louvain, Corning Incorporated, and other contributors (http://www.abinit.org).
[25] M. C. Payne, M. P. Teter, D. C. Allan, T. A. Arias, and J. D. Joannopoulos, Rev. Mod. Phys. **64**, 1045 (1992).
[26] S. Goedecker, SIAM J. Sci. Comput. (USA) **18**, 1605 (1997).
[27] J. P. Perdew, K. Burke, and M. Ernzerhof, Phys. Rev. Lett. **77**, 3865 (1996).
[28] C. G. Broyden, Math. Comput. **19**, 577 (1965).
[29] D. D. Johnson, Phys. Rev. B **38**, 12 807 (1988).
[30] V. Timoshevskii, D. Connetable, and X. Blase, Appl. Phys. Lett. **80**, 1385 (2002).
[31] R. L. Johnson and J. Reichardt, Nucl. Instrum. Methods Phys. Res. **208**, 791 (1983).
[32] Z. W. Lu, S.-H. Wei, and A. Zunger, Phys. Rev. B **44**, 10 470 (1991).
[33] P. Wouda, M. Schmid, B. Nieuwenhuys, and P. Varga, Surf. Sci. **417**, 292 (1998).
[34] L. Vitos, A. V. Ruban, H. L. Skriver, and J. Kollar, Surf. Sci. **411**, 186 (1998).
[35] D.-S. Wang, A. J. Freeman, and H. Krakauer, Phys. Rev. B **26**, 1340 (1982).
[36] I. Coulthard and T. K. Sham, Phys. Rev. Lett. **77**, 4824 (1996).